



Impact of excavation damage on the thermo-hydro-mechanical properties of natural Boom Clay

Linh-Quyen Dao, Yu-Jun Cui, Anh Minh A.M. Tang, Jean-Michel Pereira,
Xiang-Ling Li, Xavier Sillen

► To cite this version:

Linh-Quyen Dao, Yu-Jun Cui, Anh Minh A.M. Tang, Jean-Michel Pereira, Xiang-Ling Li, et al.. Impact of excavation damage on the thermo-hydro-mechanical properties of natural Boom Clay. Engineering Geology, 2015, 195, pp.196-205. <10.1016/j.enggeo.2015.06.011>. <hal-01271302>

HAL Id: hal-01271302

<https://enpc.hal.science/hal-01271302v1>

Submitted on 25 Apr 2018

HAL is a multi-disciplinary open access archive for the deposit and dissemination of scientific research documents, whether they are published or not. The documents may come from teaching and research institutions in France or abroad, or from public or private research centers.

L'archive ouverte pluridisciplinaire **HAL**, est destinée au dépôt et à la diffusion de documents scientifiques de niveau recherche, publiés ou non, émanant des établissements d'enseignement et de recherche français ou étrangers, des laboratoires publics ou privés.



HAL Authorization

Impact of excavation damage on the thermo-hydro-mechanical properties of natural Boom Clay

Linh-Quyen DAO ¹, Yu-Jun CUI ¹, Anh-Minh TANG ¹, Jean-Michel PEREIRA ¹, Xiang-Ling LI ², Xavier SILLEN ³

¹ Ecole des Ponts ParisTech, Navier/CERMES, Marne la Vallée, France

² European Underground Research Infrastructure for Disposal of nuclear waste In Clay Environment, ESV EURIDICE GIE, Mol, Belgium

³ Belgian Agency for Radioactive Waste and Enriched Fissile Materials (ONDRAF/NIRAS), Brussels, Belgium

Corresponding author:

Prof. Yu-Jun CUI

Ecole des Ponts ParisTech

6-8 av. Blaise Pascal, Cité Descartes, Champs-sur-Marne

77455 Marne-la-Vallée cedex 2

France

Email: yujun.cui@enpc.fr

Phone: +33 1 64 15 35 50

Fax: +33 1 64 15 35 62

Abstract

Boom Clay has been considered as a potential host-rock for the geological radioactive waste disposal in Belgium. In this context, it is important to well understand its thermo-hydro-mechanical behaviour around the disposal galleries. In this study, the effect of excavation damage on the thermo-hydro-mechanical properties of natural Boom Clay around the Connecting gallery (excavated in 2002) in the Mol underground Research Laboratory HADES (High-Activity Disposal Experimental Site) was investigated. Several samples taken from a horizontal borehole drilled in July 2012 were tested. The thermal conductivity in three different orientations (perpendicular, parallel, and 45° to the bedding plane) were measured using the needle probe method. The results show a cross-anisotropy of natural Boom Clay and an impact of the excavation damage on the thermal property of samples near the gallery. To further investigate the anisotropy behaviour, bender element tests were carried out under unconfined conditions to determine the small-strain shear modulus also in three different orientations. The obtained results confirm the anisotropic behaviour of Boom Clay. Moreover, the evolution of small-strain modulus with the distance from the gallery axis (r) was found to be similar to that of thermal conductivity: the values in the zone near the gallery are lower than those in the far field. From these experimental data, an extent of the excavation damaged zone (EDZ) of 4 m from the connecting gallery axis was determined. Further investigations on the microstructure of several samples taken at different distances r by mercury intrusion porosimetry (MIP) and scanning electron microscope (SEM) methods were carried out. Macro-pores of diameter $\geq 5 \mu\text{m}$ were identified in the samples near the gallery. The identified macro-pores were related to the effect of excavation damage, and a damage variable was thus defined, allowing a damage model to be developed. The values of the two model parameters have been determined from the observed relationship between macro-porosity and thermal conductivity. Comparisons between predicted and experimental results in terms of small strain shear modulus and hydraulic conductivity have shown reasonable agreement.

Keywords: Boom Clay; excavation damage; thermal conductivity, shear modulus, microstructure; anisotropy

65 **1. Introduction**

66 Geological formation of stiff clays or Claystone is often considered as potential host formation for the
 67 radioactive waste disposal at great depth. In Europe, several Underground Research Laboratories (URLs)
 68 have been constructed in stiff clay/Claystone formations such as the HADES URL (Belgium) in Boom
 69 Clay, Mont Terri URL (Switzerland) in Opalinus Clay, Bure URL (France) in Callovo-Oxfordian Claystone,
 70 etc. In this context, the damaged or disturbed zone around the gallery due to excavation is one of the most
 71 important research issues. This zone has several names and definitions depending on the research
 72 programs (Lanyon, 2011). According to Tsang and Bernier (2004), Tsang et al. (2005), Bastiaens et al.
 73 (2007), and Lanyon (2011), this zone is defined as the excavation damaged zone (EDZ) where the hydro-
 74 mechanical and geochemical modifications induced by the excavation lead to significant changes in flow
 75 and transport properties. For instance, these changes can be characterised by an increase of several
 76 magnitudes in hydraulic conductivity.

77 The characterisation of EDZ was investigated experimentally for several host formations such as Boom
 78 Clay (Mertens et al., 2004), Callovo-Oxfordian Claystone (Armand et al., 2007), Opalinus Clay (Popp et
 79 al., 2008). Depending on the host formation properties, time and budget, the characterisation method can
 80 be different (Lanyon, 2011). In order to investigate the fractures/damage induced by excavation and the
 81 lithology changes, borehole core drilling and logging are often used. The extent of EDZ can be identified
 82 by the changes in matrix geophysical and hydromechanical properties that are determined by the tests on
 83 the borehole cores. For instance, Matray et al. (2007) determined the EDZ extent in Tournemire's argillite
 84 (France) through changes in degree of saturation; Autio et al. (1998) did that in Äspö Hard Rock (Sweden)
 85 through changes in porosity.

86 During the excavation of Connecting Gallery (diameter 4.8 m) in HADES URL, fractures were intensively
 87 investigated. (Bastiaens et al., 2003; Mertens et al., 2004). The fracture pattern consists of two conjugated
 88 curved planes and the extent of the fractured zone in the horizontal direction is larger than that in the
 89 vertical one. Two cored borings, one horizontal and one vertical, were performed shortly after the
 90 construction of the Connecting gallery to assess the radial extent of the fractures. Fractures presumably
 91 related to the excavation were found up to about 1 metre in the horizontal core and up to about 0.6 m in the
 92 vertical core (Bernier et al., 2006). Charlier et al. (2010) analysed the extent of plastic zone developed
 93 around the gallery of PRACLAY (diameter 2.5m) at the end of excavation through numerical simulations in
 94 2D, axisymmetric and 3D conditions, and the obtained results are in good agreement with the field
 95 observation: depending on the values adopted for the parameters of the constitutive model, the calculated
 96 plastic zone can extend up to about 3 m in the vertical direction and about 10 m in the horizontal direction
 97 when considering material anisotropy.

98 Mertens et al. (2004) reported a seismic campaign performed in two parallel horizontal boreholes 2000–4
 99 and 2000–5 in the Mounting Chamber from the Connecting gallery of the HADES URL in order to identify

the extent of EDZ. These two boreholes have a distance of 3.6 m from each other. The velocity of compression wave V_p was measured using a mini-sonic probe. Significant data scatter was observed in the zone up to about 2 m from the gallery extrados, i.e. the outer surface of the gallery's wall (2.8 m in 2000–4 and 1 m in 2000–5), suggesting significant damage of this zone.

Another in-situ measure allowing the characterisation of the EDZ around the Connecting gallery is the hydraulic conductivity (k). Yu et al. (2011a) reported a large investigation over 30 years on the hydraulic conductivity of Boom Clay. Some data involve the evolution of hydraulic conductivity with the distance from the gallery extrados. For instance, two piezometers equipped with pressure controller and high-definition balance were installed: R55D (vertical) and R55E (horizontal). The measurement obtained from the vertical piezometer is mainly the contribution of k_h or $k_{//}$ (hydraulic conductivity parallel to the bedding plane), while the measurement obtained from the horizontal piezometer (k_g) is the combined contribution of k_{\perp} (hydraulic conductivity perpendicular to the bedding plane) and $k_{//}$ (Yu et al., 2013a). The relation between k_g , k_{\perp} and $k_{//}$ after Roy (1991) is:

$$k_g = \sqrt{k_{\perp} \cdot k_{//}} \quad (1)$$

Using Eq. (1), the vertical hydraulic conductivity can be deduced using the measurements from the vertical and horizontal piezometers. The obtained results show that the hydraulic conductivity is strongly disturbed in the zone of 6 m from the gallery's wall. This extent is larger than that deduced from V_p measurements (2 m from the gallery's wall).

Several studies showed that the EDZ in Boom Clay can be sealed after a certain time, with a hydraulic behaviour that becomes close to that of intact Boom Clay (Bastiaens et al., 2007; Mertens et al., 2002). On the other hand, healing, i.e. restoration of original mechanical properties, has not been demonstrated. This aspect was investigated in this study by testing Boom Clay cores taken 10 years after the gallery excavation (2002). The EDZ extent was appreciated based on changes in small-strain shear modulus (G_0) and thermal conductivity (λ). Different directions with respect to the bedding plane were considered, allowing the anisotropic behaviour to be studied. Furthermore, microstructure changes were also analysed, allowing identification of the creation of a population of macro-pores that was due to the excavation damage. A parameter related to these macro-pores was then defined, allowing description of the effect of excavation damage on the thermo-hydro-mechanical properties (i.e. thermal conductivity - λ , small-strain shear modulus - G_0 and hydraulic conductivity - k) of Boom Clay.

2. Materials and methods

2.1. Materials

Boom Clay is located in the North of Belgium at depth between 185 m and 287 m at Mol (Mertens et al., 2004). Its bedding plane is considered to be almost horizontal; its layer is gently dipping ($\pm 1^\circ$) toward the North-North-East (Mertens et al. 2003). This material mainly consists of clay minerals dominated by

kaolinite and illite (Lima, 2011, Dehandschutter et al., 2005). In this study, several samples were taken from a horizontal borehole (R66-67) of 100 mm diameter (the axis is parallel to the bedding plane). This borehole was drilled in July 2012 from the connecting gallery which was excavated in 2002 with 4.0 m diameter and 0.4 m thick liner. The full code of the borehole or cores is: Boom Clay / Mol Site / HADES borehole 2012-2 / Connecting gallery / Ring 66-67W / 0.40 m to 20.3 m from the intrados of the lining. After being extracted, each core sample was vacuum-packaged in aluminium foil to minimise water loss by evaporation.

The initial suction of Boom Clay after opening these aluminium foils was measured using a dew-point hygrometer and a value of about 3 MPa was obtained which is close to that estimated by Delage et al. (2007). Other parameters such as water content (w), degree of saturation (S_r) were also measured. Further examination shows that the relationship between suction and water content was in good agreement with the retention curve reported by Delage et al. (2007).

2.2. Thermal conductivity measurement

After trimming from core, the samples (100 mm in diameter and 60 mm - 90 mm in height) were then slightly confined by means of an adhesive tape so as to avoid further crack propagation and any perturbation. The thermal conductivities of natural Boom Clay in three orientations (parallel, perpendicular and 45° to the bedding plane) were measured using a thermal needle probe - KD2 Pro. A single needle (60 mm in length, 1.3 mm in diameter) was inserted into the soil specimen (Figure 1). In this needle probe method (or line source method), the theory of axisymmetric heat diffusion from an infinite line source within an infinite surrounding medium was used. Hence, a radial heat flow is produced within the specimen while measuring temperature changes over time. More details can be seen in Tang et al. (2008). In order to measure the thermal conductivity in three orientations, three holes were drilled in each sample in order to vary the angle θ between the axis of needle probe and the bedding plane ($\theta = 0^\circ, 45^\circ, 90^\circ$) (see Figure 1). Note that in the case of $\theta = 90^\circ$, the measured thermal conductivity λ_{90} is not the value in the direction perpendicular to the bedding plane (λ_\perp). The true value of λ_\perp is back-calculated from $\lambda_{//}$ (or λ_0) and the apparent thermal conductivity λ_{90} using Eq. (2) (Penner, 1963):

$$\lambda_\perp = \frac{(\lambda_{90})^2}{\lambda_0} \quad (2)$$

As the samples used were at unsaturated state, Johansen's method (Farouki, 1986) for fine unfrozen soils was used to calculate the thermal conductivity at saturated state (λ_{sat}) from the thermal conductivity at unsaturated state (λ) and dry state (λ_{dry}) (Eq. (3)):

$$\lambda_{sat} = \frac{(\lambda - \lambda_{dry})}{K_e} + \lambda_{dry} \quad (3)$$

where

$$K_e \cong \log S_r + 1.0 \quad (4)$$

$$\lambda_{dry} = \frac{0.135\gamma_d + 64.7}{2700 - 0.947\gamma_d} \pm 20\% \text{ (W / mK)} \quad (5)$$

where γ_d is the dry density expressed in kg/m³.

2.3. Shear modulus measurement

The small-strain shear modulus (G_0) in different orientations of natural Boom Clay was determined by performing bender elements tests under unconfined conditions. In a bender element test, the velocity of shear wave (V_s) is determined allowing calculation of the small-strain shear modulus (G_0). The experimental set-up used is depicted in Figure 2 (only soil sample and the transmitter are presented). The receiver placed under the soil sample is not sketched in this figure.

For each sample (100 mm in diameter and 55 mm - 80 mm in height), the shear wave in three different orientations (V_{hv} , V_{hh} , V_{h45}) were generated by letting vibrate the transmitter element in the direction perpendicular, parallel and at 45° with respect to the bedding plane. Note also that the direction of wave propagation is always parallel to the bedding (see Figure 2). The travel times (Δt) of shear wave was determined. Then three small-strain shear modulus G_{hv} , G_{hh} , G_{h45} were calculated using Eq. (6) (Zeng and Ni, 1999):

$$G_{0(ij)} = \rho V_{s(ij)}^2 \quad (6)$$

where i and j are the directions of shear wave propagation and particle vibration in the σ_1 - σ_1 plane, respectively; ρ is the total density of soil (Mg/m³); G_0 is small-strain shear modulus (kPa), V_s is shear wave velocity (m/s) determined by Eq. (7):

$$V_s = \frac{l}{\Delta t} \quad (7)$$

where l is the travel length of shear wave.

Note that the samples used for the bender element tests were the same as those used in the thermal conductivity tests. Note also that the water content in these cores slightly decreased during the conservation in the laboratory, resulting in an increase in suction. The values range from 3 MPa (suction measured during thermal conductivity tests) to 5 MPa (suction measured during the bender element tests).

2.4. Microstructural investigations

Two microstructural observation methods were used: scanning Electron Microscopy (SEM) and Mercury Intrusion Porosimetry (MIP). Note that the samples were freeze-dried prior to observations to minimise the modification of soil microstructure (Delage and Pellerin, 1984). The MIP tests were performed on an “AutoPore IV 9500 – Micromeritics Instrument Corp”. This equipment has two stages of pressure application. In the first stage, the equipment performs mercury intrusion at low pressures in the range between 0.0035 and 0.2 MPa, and measuring apparent pore diameters between 400 μm and 3 μm . In the second stage, the high-pressure is applied between 0.2 and 227.5 MPa, measuring pores diameters ranging from 3 μm to 0.005 μm .

3. Experimental results

3.1. Shear stiffness and thermal conductivity

The variations of G_{hv} , G_{h45} , G_{hh} with the distance r from the axis of gallery for each sample are presented in Figure 3. It appears that G_{hh} displays a clear trend with distance r : It stabilises at 1450 MPa in the zone far from the gallery, decreases to 1200 MPa at $r = 4$ m and then drops to 800 MPa at $r = 2.5$ m. For G_{hv} , except two values (638 MPa at $r = 2.7$ m and 1403 MPa at $r = 3.8$ m), a significant decrease is identified from the far field (1200 MPa at $r = 9.2$ m) to the near field (808 MPa at $r = 2.5$ m). The value of G_{hv} at $r = 16$ m is equal to the value of G_{hh} . This is quite surprising because G_{hv} is expected to be lower than G_{hh} due to the cross-anisotropy of Boom Clay formation. For G_{h45} , except two values at $r = 4$ m (1098 MPa) and $r = 16$ m (1009 MPa), it seems to stabilise around 1300 MPa at the distance r from 3.8 m to 9.2 m, then decreases to 1066 MPa at $r = 2.5$ m. In spite of the irregular evolutions of G_{hv} and G_{h45} , it appears clearly that the shear stiffness of the zone near the gallery $r < 4$ m (about 1.6 m from the gallery extrados) is lower than that in the far field. It is also found that the obtained values of G_{hv} and G_{hh} in the far field are in good agreement with those obtained by Lima (2011) under unconfined condition ($G_{hh} = 1483$ MPa and $G_{vh} = 1135$ MPa). Areias et al. (2012) also measured the shear wave velocity in the field and obtained a value of V_s around 800 m/s that corresponds to a value of G_0 of 1280 MPa. This is in agreement with the value obtained in this study.

The results of thermal conductivity at saturated state in the directions parallel ($\lambda_{//}$ measured), perpendicular (λ_{\perp} calculated) and 45° (λ_{45} measured) to the bedding plane are shown in Figure 4 versus the distance r from the axis of gallery. For the $\lambda_{//}$ measured, the value stabilises at 1.6 W/(m.K) in the zone far from the gallery then drops to 1.46 W/(m.K) at $r = 3.4$ m and afterwards quickly decreases to 1.3 W/(m.K) at $r = 2.5$ m. The value of $\lambda_{//}$ in the far field ($r > 4$ m) is close to that found by Chen et al. (2011) by back analysis of a metre-scale in situ heater test (1.65 W/(m.K)). The variation trend of λ_{45} is similar to that of $\lambda_{//}$: the value stabilises at 1.5 W/(m.K) then quickly decreases to 1.2 W/(m.K) at $r = 2.5$ m. For λ_{\perp} calculated, the variation is not as regular as for $\lambda_{//}$ and λ_{45} : the value in the far field varies slightly between 0.95 and 1.05 W/(m.K), drops down to 0.8 W/(m.K) at $r = 2.7$ m then increases to 0.9 W/(m.K) at $r = 2.5$ m. From the measurements of thermal conductivity and small-strain shear modulus, the lasting influence of

excavation damage is confirmed, even more than 10 years after the excavation, at least on thermal-mechanical properties of unconfined samples.

3.2. Microstructural investigation

Mercury Intrusion Porosity (MIP) and Scanning Electron Microscopy (SEM) tests were carried out on several Boom Clay samples located at three distances r (2.5 m, 2.7 m and 9.2 m) to the gallery axis. The microstructural investigations were performed after measuring the thermal conductivity and the shear modulus. The bedding plane of Boom Clay can be detected at macroscopic scale as shown in Figure 5. The physical properties of Boom Clay samples used for MIP and SEM tests can be found in Table 1. Figure 6 shows the pore size distribution curves for the three samples. From pore size 5 nm to 5000 nm (i.e. 5 μm), the curves have a similar shape (Figure 6a) with a well-defined pore population at 80 nm. This observation is consistent with that by Lima (2011) and Nguyen (2013). The curves also revealed that these samples have almost no pores in the range from 1 μm and 5 μm . However, for the range beyond 5 μm , the two samples located near the gallery's wall ($r = 2.5$ m and $r = 2.7$ m respectively) show the presence of macro-pores, with the macro-pores being more pronounced for the sample which is closest to the gallery - $r = 2.5$ m. These macro-pores could be related to the fissures created by the gallery excavation or to the excavation damage. It is also observed from Figure 6b that the final value of the intruded mercury void ratio (mercury intruded volume/volume of soil particles) for the three samples are always lower than their corresponding global soil void ratio e (see Table 1) due to non-intruded porosity (Lima, 2011).

To further evaluate the soil behaviour at microscopic level, the intruded mercury void ratio of macro-pore e_M is used, which is the ratio of the mercury intruded volume of macro pore V_M to the volume of soil particles V_s (Eq. (8)):

$$e_M = \frac{V_M}{V_s} \quad (8)$$

The e_M of the Boom Clay samples is estimated by using the curves $e_M - D$ (Figure 6b). For the three samples tested: $e_M = 0.05$ ($r = 2.5$ m); $e_M = 0.02$ ($r = 2.7$ m); $e_M = 0.01$ ($r = 9.2$ m). Figure 7 shows the evolution of e_M with distance r . It can be observed that the nearest sample to the gallery ($r = 2.5$ m) has the maximum value of e_M , and the sample at $r = 9.2$ m has the minimum.

The pore size distribution analysis was completed by the SEM observation. The views perpendicular and parallel to the bedding plane for the samples taken from three different distances, $r = 2.5$ m, 2.7 m and 9.2 m, are shown in Figure 8, Figure 9 and Figure 10, respectively. For the sample located at $r = 2.5$ m, two photographs were taken at two dimensions: 1800 x 1400 μm (Figure 8a), 1500 x 1100 μm (Figure 8b). In Figure 8a, the beam of electron of microscope being parallel to the bedding plane, the bedding plane was clearly identified. In addition, a crack of about 50 μm wide parallel to the bedding plane is detected. In Figure 8b, the beam of electron of microscope being perpendicular to the bedding plane, hence several

clay platelets parallel to each other are observed, without the presence of large cracks. From the pore size distribution curve at $r = 2.5$ m (Figure 6a), macro-pores are observed in the range from 10 μm to 100 μm . The crack identified in Figure 8a corresponds to these identified macro-pores.

The SEM photographs of the second sample located at $r = 2.7$ m are presented in Figure 9. When focusing the beam of electron parallel to the bedding plane (Figure 9a), the bedding plane is still well detected. Moreover, a crack as large as 40 μm and parallel to the bedding plane is also observed. In Figure 9b, as the dimensions picture are smaller (850 x 650 μm) than that of Figure 8b, clay platelets are identified more clearly: they are superimposed upon each other. For this sample, the pore size distribution curve (Figure 6a) also shows some macro-pores of 10 μm to 100 μm . This is also in good agreement with the crack observed in Figure 9a.

For the sample located far from the gallery ($r = 9.2$ m), two photographs at two scales were taken: 2300 x 1800 μm (Figure 10a with the beam of electron parallel to the bedding plane) and 640 x 500 μm (Figure 10b with the beam of electron perpendicular to the bedding plane). Although the dimensions of Figure 10a are close to those of Figure 6a and Figure 8a, only the bedding plane is detected and no crack is found. As the dimension of Figure 10b is slightly smaller than that of Figure 9b, several bedding planes are clearly observed.

Summarising, there is a good agreement between the MIP and SEM analyses, suggesting that the void ratio of macro-pore e_M (diameter ≥ 5 μm) is due to excavation damage. In other words, the excavation damage zone still exists even more than 10 years after the excavation. There are certainly some desiccation cracks after the sample has been taken out of the borehole. But the others results on Boom Clay samples at the “perfect” state (far field and undamaged condition) didn’t show the cracks with the same dimension and density.

4. Prediction of thermo-hydro-mechanical properties

4.1. Damage variable

Many theories of continuous damage mechanics were developed based on the concept of effective stress of Kachanov (1958) (see (Ambroziak, 2007; Gross and Seelig, 2011)). It is assumed that the relationship between the effective stress in the damaged material (σ_{ij}^*) and that of the undamaged material (σ_{ij}) is defined by a damage variable D (Eq. (9)):

$$\sigma_{ij}^* = \frac{\sigma_{ij}}{1-D} \quad (9)$$

For a linear elastic material, the amount of damage can be determined by Eq. (10):

$$D = 1 - \frac{E^*}{E} \quad (10)$$

where E is the Young's modulus of undamaged material, E^* is the Young modulus of damaged material.

In this study, as a decrease of thermal conductivity and small-strain shear modulus has been identified in the location near the galley and this decrease is related to the excavation damage characterised by the creation of macro-pores, a semi-empirical expression can be proposed to estimate the effect of excavation damage on the properties of Boom Clay (see Eq. (11)). In this expression, parameter e_M defined by the pores larger than 5 μm is used as a measure of damage levels:

$$X = X_0 (1 - b \exp(-a \frac{e}{e_M})) \quad (11)$$

where X_0 is the property of Boom Clay in the far field (intact zone), X is the property of Boom Clay in the near field (EDZ), e is the global void ratio (see Table 1). In this empirical equation, the damage variable considered is the ratio between e and e_M .

In Eq. (11), there are two parameters to be determined: $a > 0$ is a parameter depending on the material and b is a parameter depending on the property considered ($b > 0$ if the property of material decreases with the increase of macro-pores; $b < 0$ if the property of material increases with the increase of macro-pores). Note that the derived fitting parameters a and b have no physical meaning. They just serve to get a good agreement between the laboratory or field values and the modelled values. Thus, this modelling is not based on hydraulic and/or mechanical processes.

4.2. Determination of parameters

For Boom Clay, the results of thermal conductivity measurements are used to determine the two parameters a and b by comparing the modelled and experimental results. For this purpose, the values of λ_{\perp} , λ_{45} , λ_{\parallel} in the far field (1.1 W/(m.K), 1.5 W/(m.K), 1.65 W/(m.K) respectively, see Table 2) are chosen to compute the thermal conductivity at three distance $r = 2.5$ m, 2.7 m and 9.2 m. With $a = 0.05$ and $b = 0.5$, a good agreement is obtained between the model prediction and experimental results (Figure 4).

The same model is used to predict the small-strain shear modulus (G_{hv} , G_{h45} , G_{hh}) located at three different distances: $r = 2.5$ m, 2.7 m and 9.2 m. As for the thermal conductivity, the values of G_{hv} , G_{h45} , G_{hh} in the intact zone and presented in Table 2 are used in the calculations. The predicted results with the same parameters ($a = 0.05$ and $b = 0.5$) are compared to that measured in the laboratory in Figure 3. A good agreement is also obtained. Note that the experimental values of thermal conductivity and small-strain shear modulus at these three distances r are presented in Table 1.

4.3. Application of the damage model to the hydraulic property

In order to verify this damage model for the hydraulic property of natural Boom Clay, the field hydraulic conductivity measurements in 2004 and 2005 (reported by Yu et al., 2011) and those obtained from the same piezometers R55D and R55E in 2012 (taken from the internal report of EURIDICE) are analysed.

The results of hydraulic conductivity k measurements in 2004, 2005 and 2012 are presented in Figure 11. Due to the excavation damage in the zone near the gallery, the hydraulic conductivity is quite high in this zone. The extent of EDZ, where the hydraulic conductivity is disturbed, reaches 6 m from the gallery extrados. Out of the EDZ, the values are about $6.5 \cdot 10^{-12}$ m/s for $k_{//}$ and at $3.5 \cdot 10^{-12}$ m/s for k_{\perp} (computed from k_g and $k_{//}$ using Eq. (1)). Comparison between the results of 2004, 2005 and 2012 shows that the influence of excavation on the hydraulic conductivity in the direction parallel to the bedding plane ($k_{//}$) in 2004 is the same as that in 2005 but larger than that in 2012, which suggests that self-sealing was still in progress from 2005 to 2012. In terms of geometric hydraulic conductivity k_g , the results measured in 2004 are almost identical to those obtained in 2005 and 2012.

To apply the proposed damage model to the hydraulic conductivity, parameter a is taken the same as that used for the predictions of thermal conductivity and small strain shear modulus. By contrast, parameter b is taken equal to -0.5 because the hydraulic conductivity increases with the increase of macro-pores. All the calculated values (k_{\perp} , $k_{//}$) are then compared to those measured in situ (Figure 11). It is observed that the predicted results are closer to those of the measurements of 2012 as compared with the measurements of 2004 and 2005. This is logic because the values of e_M are determined on samples taken in 2012.

The good agreement obtained between the model prediction and experimental data for the thermal conductivity (Figure 3), small-strain shear modulus (Figure 4) and hydraulic conductivity (Figure 11) shows that the damage variable defined based on the volume of macro-pores is relevant in predicting the effect of EDZ on the thermo-hydro-mechanical properties of natural Boom Clay.

5. Discussion

Experimental methods aiming at understanding the properties of stiff clay/soft rock in the EDZ often rely on in-situ identification, such as the ultrasonic velocity measurement used for Callovo-Oxfordian claystone (Schuster and Alheid, 2007), Boom Clay (Mertens et al., 2004), and Opalinus Clay (Martin Derek et al., 2003), the hydraulic conductivity measurement used for Boom Clay (Yu et al., 2011), Opalinus Clay (Martin Derek et al., 2003), etc. In this study, the measurements of small-strain shear modulus (G_0) and of thermal conductivity (λ) were undertaken in the laboratory to quantify the extent of EDZ in Boom Clay. From these measurements, it has been observed that the experimental data of λ and G_0 follows the same evolution law with the distance r from the gallery. -. By contrast, within the EDZ, there is a drastic decrease in its hydro-mechanical performance. This is confirmed by the evolution of hydraulic property reported by Yu et al. (2011): a higher value was obtained in the EDZ as compared to the zone outside the EDZ. The presence of EDZ around Boom Clay formation was also confirmed through the in-situ measurement of compressional wave velocity (V_p) by Mertens et al. (2004). Unfortunately, the boreholes

used to measure V_p in the study of Mertens et al. (2004) are not perpendicular to the connecting gallery, thus the interpretation of data is not straightforward.

As for the experimental methods of EDZ identification, the fracture/damage induced by excavation can be identified by mapping excavation surfaces (Lanyon, 2011). Following up this method, a method of tunnel crossing excavation that cut into the side-wall of the previously excavated tunnels was used (Martin and Lanyon, 2004) to detect the extent of EDZ in Opalinus Clay. As for the numerical approaches, there are several methods to predict the extent of EDZ using finite elements, explicit finite difference, distinct element, etc. To simulate the soil damage (fracture growth), a damage variable (usually called D) is used which is derived from the test results of axial stress and strain, tangential strain, Young's modulus and Poisson's ratio (Hudson, 2009). In this study, the fractures which have the plate and parallel opening form observed at a microscopic scale were considered. Firstly, the global void ratio (e) of the samples taken near and far the gallery was checked to detect the influence of fractures due to excavation on e_0 . Table 1 shows that the values of e of the three samples are almost the same, suggesting that e_0 is not an indicator of excavation damage. Then, the microstructure investigation of these samples was carried out, allowing the definition of a relevant damage parameter that is the ratio of the global void ratio (e_0) to the void ratio of macro-pores (pore diameter $\geq 5 \mu\text{m}$) (e_M). When the soil is in the EDZ, there are more macro-pores, giving rise to larger values of e_M . Note that the applicability of this model is related to crack form openings. When the lower damage limit is reached (i.e. undamaged state), the value of e_M is very small and X is considered to be equal to X_0 . When the upper damage limit is reached (i.e. totally damaged state), the value of e_M is very high and $e/e_M \approx 0$, hence $X \approx 0$.

As the values of e_0 for all the three samples are around 0.64, the damage variable (e/e_M) depend only on e_M .

Figure 3, Figure 4, and Figure 11 show some differences between the experimental and prediction results. These differences are due to the chosen values of parameters a and b and the far field values of thermal conductivity, small-strain modulus and hydraulic conductivity (Table 2). In terms of thermal conductivity, the chosen far field values of $\lambda_{//}$ (1.65 W/(m.K)) and λ_{45} (1.5 W/(m.K)) allow the predictions close to the experimental data. But for λ_{\perp} , the trend of experimental data is not regular due to the low values measured on the samples of far field: it increases to 1.05 W/(m.K) at $r = 6.0$ m then decreases to 0.95 W/(m.K) at $r = 20.8$ m. Comparing to the value of $\lambda_{\perp} = 1.31$ W/(m.K) obtained by Chen et al. (2011) by back-analysis, a far field value of $\lambda_{\perp} = 1.1$ W/(m.K) was chosen.

In the case of small-strain modulus, the far field values of G_{hv} , G_{h45} , G_{hh} are more difficult to choose because the measurements by bender element always show some experimental data scatters. Among the three parameters measured (V_{hv} , V_{hh} and V_{h45}), it seems that V_{h45} is the most difficult to measure. There are several sources that may affect the accuracy of the measurement: identification of the bedding plane, contact between transmitter/receiver and the soil specimen, etc. The final far field values of G_{hv} , G_{h45} , G_{hh} were chosen after comparing the measurements in this study and the values proposed by Lima (2011) under unconfined conditions.

In terms of hydraulic conductivity, the in-situ data showed the far field value clearly, but the predicted results under-estimate the values in EDZ, especially in the case parallel to the bedding plane $k_{//}$ with the measurements conducted in 2004 and 2005 (Figure 11). As mentioned before, this is because parameters a and b are determined based on the measurements on the samples from the borehole drilled in July 2012, with the values of e_M that must be lower than those in 2004 and 2005, due to the self-sealing capacity of Boom Clay. The decrease of e_M over time is related to the decrease of the dimensions of cracks identified in Figures 8 and 9. The large difference between the predicted results and the data of 2004 and 2005 shows that parameters a and b change over time. In other words, a given set of parameters corresponds to a given time, and the proposed model can be used to estimate the effect of EDZ only for this given time.

6. Conclusions

This study aimed at investigating the influence of EDZ around the connecting gallery on the thermal conductivity, small strain modulus and hydraulic conductivity. Several samples of natural Boom Clay at different distances from the gallery were taken from the borecore drilled in July 2012, and thermal conductivity and bender element tests were carried out on these samples. As Boom Clay is a cross-anisotropic material, the anisotropy of its properties was investigated by considering different directions with respect to the bedding plane. Microstructural observations were also made using MIP and SEM methods on the samples located at different distances from the gallery. The identified macro-pores were related to the effect of excavation damage, and a damage variable was thus defined, allowing the properties of Boom Clay to be estimated.

In terms of thermal measurements, the thermal conductivity (λ) in three directions - parallel ($\lambda_{//}$), perpendicular (λ_{\perp}), and inclined 45° (λ_{45}) to the bedding plane was measured using the needle probe method. The results showed the same evolution with the distance r from the gallery axis in the three orientations: in the zone far from the gallery, the thermal conductivity stabilises then it drops down to lower values while $r < 4$ m. An extent of EDZ about 4 m from the gallery axis (1.6 m from the gallery extrados) was identified.

The mechanical property of Boom Clay around the connecting gallery was investigated through the measurements of the small-strain shear modulus (G_0) by bender element under unconfined conditions. The values in three directions G_{hv} , G_{h45} , G_{hh} were determined on samples at several distances r . Although the experimental results are not as regular as those for the thermal conductivity, an extent of EDZ of about 4 m from the gallery axis was also identified.

The MIP tests revealed that the samples close to the gallery's wall have macro-pores larger than $5 \mu\text{m}$. These pores correspond to cracks observed at the SEM observations, and can be related to the excavation damage.

From the void ratio of macro-pore e_M obtained from the MIP tests, a damage variable was defined and a damage model was proposed allowing the prediction of the thermal-hydro-mechanical properties of Boom Clay around the gallery. This model was validated by comparing the predicted and experimental results in terms of thermal conductivity and small-strain shear modulus in different orientations, with the same parameters a and b . Further analysis was conducted in terms of hydraulic conductivity. It was observed that satisfactory prediction was obtained for the year 2012 where both the hydraulic conductivity measurement and the sampling for e_M determination were done. The results also suggest that parameters a and b may change over time because of the self-sealing capacity of Boom Clay that leads to a decrease of e_M over time.

Acknowledgements

The authors would like to express their gratitude to Ecole des Ponts ParisTech (ENPC), European Underground Research Infrastructure for Disposal of nuclear waste In Clay Environment (EURIDICE) and Belgian Agency for Radioactive Waste and Enriched Fissile Materials (ONDRAF/NIRAS) for their financial supports.

References

- Ambroziak, A., 2007. Identification and validation of damage parameters for elsto-viscoplastic chaboche model. Eng. Trans. 55, 3–28.
- Areias, L., Verstricht, J., Fischer, T., Philipp, J., 2012. Seismic Monitoring at the Underground Nuclear Research Laboratory in MOL, Belgium - 12461, in: WM2012 Conference. Phoenix, Arizona, USA.
- Armand, G., Lebon, P., Cruchaudet, M., Rebours, H., Morel, J., Wileveau, Y., Agence, A.-, De, L., Meuse, D., Marne, H., Cedex, C., 2007. EDZ Characterisation in the Meuse / Haute-Marne Underground Research Laboratory, in: Clays in Natural & Engineered Barriers for Radioactive Waste Confinement. International meeting, September 17-18 2007, Lille, France, pp. 153–154.
- Autio, J., Siitari-Kauppi, M., Timonenc, J., Hartikainen, K., Hartikainen, J., 1998. Determination of the porosity, permeability and diffusivity of rock in the excavation-disturbed zone around full-scale deposition holes using the View the C14-PMMA and He-gas methods. J. Contam. Hydrol. 35, 19–29.
- Bastiaens, W., Bernier, F., Buyens, M., Demarche, M., Li, X.L., Linotte, J.M. and Verstricht, J., 2003. The Connecting Gallery - the extension of the HADES underground research facility at Mol, Belgium. EURIDICE report 03-294. Mol: ESV EURIDICE.
- Bernier, F., Li, X.L., Bastiaens, W., Ortiz, L., Van Geet, M., Wouters, L., Frieg, B., Blümling, P., Desrues, J., Viaggiani, G., Coll, C., Chanchole, S., De Greef, V., Hamza, R., Malinsky, L., Vervoort, A., Vanbrabant, Y., Debecker, B., Verstraelen, J., Govaerts, A., Wevers, M., Labiouse, V., Escoffier, S., Mathier, J.F., Gastaldo, L. and Bühler, Ch., 2006. Fractures and self-healing within the excavation disturbed zone in clays. EC report on the SELFRAC project.

463 Bernier, F., Li, X.L., Bastiaens, W., 2007. Twenty-five years' geotechnical observation and testing in the
464 Tertiary Boom Clay formation. *Géotechnique* 57, 229–237.

465 Charlier, R., Collin, F., Dizier, A., Fauriel, S., Gens, A., Guangjing, C., Laloui, L., Meynet, T., Pascon, F.,
466 Radu, J.P., Marcke, P., Vaunat, J., 2010. Thermal Impact on the Damaged Zone Deliverable D13 –
467 Annex 6 Large scale excavation and heater in-situ experiment : the PRACLAY experiment
468 modelling.

469 Chen, G.J., Sillen, X., Verstricht, J., Li, X.L., 2011. ATLAS III in situ heating test in boom clay: Field data,
470 observation and interpretation. *Comput. Geotech.* 38, 683–696.

471 Das, B.M., 1983. *Advanced Soil Mechanics*. Hemisphere Publishing Corp.

472 Dehandschutter, B., Vandycke, S., Sintubin, M., Vandenberghe, N., Wouters, L., 2005. Brittle fractures
473 and ductile shear bands in argillaceous sediments: inferences from Oligocene Boom Clay (Belgium).
474 *J. Struct. Geol.* 27, 1095–1112.

475 Delage, P., Pellerin, F.M., 1984. Influence de la lyophilisation sur la structure d'une argile sensible du
476 Québec. *Clays Miner.* 19, 151–160.

477 Delage, P., Le, T.T., Tang, A.M., Cui, Y.J., Li, X.L., 2007. Suction effects in deep Boom Clay block
478 samples. *Géotechnique* 57, 239–244.

479 Diamond, S., 1970. Pore size distribution in clays. *Clays Clay Min.* 18, 7–23.

480 Farouki, O.T., 1986. *Thermal properties of soils*. Trans Tech Publications, Clausthal-Zellerfeld, Germany.

481 Gross, D., Seelig, T., 2011. Damage mechanics, in: *Fracture Mechanics SE - 9*. Springer Berlin
482 Heidelberg, pp. 301–316.

483 Hudson, J.A., 2009. Characterising and modelling the excavation damaged zone (EDZ) in crystalline
484 rock in the context of radioactive waste disposal. Lawrence Berkeley Natl. Lab.

485 Kachanov, L., 1958. Time of the rupture process under creep conditions. *TVZ Akad Nauk S.S.R Otd.*
486 *Tech. Nauk* 8, 26–31.

487 Lanyon, G., 2011. Excavation Damaged Zones Assessment, OPG's Deep Geologic Respository for Low
488 & Intermediate waste. Report of Fracture Systems Ltd - NWMO DGR-TR-2011-21.

489 Le, T.T., 2008. Comportement thermo-hydro-mécanique de l'argile de Boom. PhD. Ecole Nationale des
490 Ponts et Chaussées.

491 Lima, A., 2011. Thermo-hydro-mechanical behaviour of two deep Belgian clay formations: Boom and
492 Ypersian Clays. PhD thesis. Universitat Politècnica de Catalunya.

493 Martin, C., Lanyon, G.W., 2004. Excavation Disturbed Zone (EDZ) in Clay Shale: Mont Terri.

494 Martin Derek, C., Lanyon, G.W., Blümling, P., Mayor, J., 2003. The excavation disturbed zone around a
495 test tunnel in the Opalinus Clay. *Tunn. Assoc. Canada Annu. Publ.*

496 Matray, J.M., Savoye, S., Cabrera, J., 2007. Desaturation and structure relationships around drifts
497 excavated in the well-compacted Tournemire's argillite (Aveyron, France). *Eng. Geol.* 90, 1–16.

498 Mertens, J., Bastiaens, W., Dehandschutter, B., 2004. Characterisation of induced discontinuities in the
499 Boom Clay around the underground excavations (URF, Mol, Belgium). *Appl. Clay Sci.* 26, 413–428.

- 500 Mertens, J., Vandenberghe, N., Wouters, L., Sintubin, M., 2003. The origin and development of joints in
501 the Boom Clay Formation (Rupelian) in Belgium. *Geol. Soc. London, Spec. Publ.* 216 , 309–321.
- 502 Mertens, J., Bastiaens, W., Dehandschutter, B., 2002. Characterisation of induced discontinuities in the
503 Boom Clay around the underground excavations (URF, Mol, Belgium), in: *Clays in Natural &*
504 *Engineered Barriers for Radioactive Waste Confinement*. pp. 43–44.
- 505 Nguyen, X.P., 2013. Étude du comportement chimico-hydro- mécanique des argiles raides dans le
506 contexte du stockage de déchets radioactifs. PhD thesis. Université Paris-Est.
- 507 Penner, E., 1963. Anisotropic thermal conduction in clay sediments, in: *International Clay Conference*.
- 508 Popp, T., Salzer, K., Minkley, W., 2008. Influence of bedding planes to EDZ-evolution and the coupled HM
509 properties of Opalinus Clay. *Phys. Chem. Earth* 33, S374–S387.
- 510 Romero, E., 1999. Characterisation and thermo-hydro-mechanical behaviour of unsaturated Boom Clay:
511 An experimental study. *Universitat Politècnica de Catalunya*.
- 512 Roy, P., 1991. Measurements of soil permeability anisotropy by three techniques. Thesis. McGill
513 University (Montreal).
- 514 Schuster, K., Alheid, H.J., 2007. EDZ characterisation with ultrasonic interval velocity measurements in
515 the URL Meuse/Haute-Marne -performed between depth of 85 m and 504 m, in: *International*
516 *Meeting “Clay in Natural & Engineered Barriers for Radioactive Waste Confinement”*. September 17-
517 18, Lille, France, pp. 155–156.
- 518 Tang, A.M., Cui, Y.J., Le, T.T., 2008. A study on the thermal conductivity of compacted bentonites. *Appl.*
519 *Clay Sci.* 41, 181–189.
- 520 Tsang, C.F., Bernier, F., 2004. Definitions of excavation disturbed zone and excavation damaged zone, in
521 Impact of the excavation disturbed or damaged zone (EDZ) on the performance of radioactive waste
522 geological repositories, in: *Proceedings European Commission CLUSTER Conference and*
523 *Workshop on EDZ in Radioactive Waste Geological Repositories*. Luxembourg, Belgium.
- 524 Tsang, C.F., Bernier, F., Davies, C., 2005. Geohydromechanical processes in the Excavation Damaged
525 Zone in crystalline rock, rock salt, and indurated and plastic clays- in the context of radioactive waste
526 disposal. *Int. J. Rock Mech. Min. Sci.* 42, 109–125.
- 527 Yu, L., Gedeon, M., Wemaere, I., Marivoet, J., De Craen, M., 2011a. Boom Clay Hydraulic Conductivity. A
528 synthesis of 30 years of research. External report SCK-CEN, Mol (Belgium).
- 529 Yu, L., Weetjens, E., Vietor, T., 2011b. Integration of TIMODAZ Results within the Safety Case and
530 Recommendations for Repository Design.
- 531 Yu, L., Rogiers, B., Gedeon, M., Marivoet, J., Craen, M. De, Mallants, D., 2013. A critical review of
532 laboratory and in-situ hydraulic conductivity measurements for the Boom Clay in Belgium. *Appl. Clay*
533 *Sci.* 75-76, 1–12.
- 534 Zeng, X., Ni, B., 1999. Stress-Induced anisotropic Gmax of sands and its measurement. *J. Geotech.*
535 *Geoenvironmental Eng.* 125, 741–749.

536

537 List of Tables

538 Table 1: Physical and thermo-mechanical properties of natural Boom Clay. r : distance from the axis of
539 gallery, w : water content (%), ρ : total density of the soil, λ : thermal conductivity, G : small-strain shear
540 modulus, e : void ratio; e_M : void ratio of macro-pores.

541 Table 2: Parameters used for model predictions.

542

543 List of Figures

544 Figure 1: Measurement of thermal conductivity by needle probe method in the laboratory.

545 Figure 2: Measurement of shear wave velocity by bender element method in the laboratory (the three
546 arrows indicate the directions of particle vibration).

547 Figure 3: Comparison of shear modulus between model and experiment.

548 Figure 4: Comparison of thermal conductivity between model and experiment.

549 Figure 5: Bedding plane on natural Boom Clay sample.

550 Figure 6: Pore size distributions of three Boom Clay samples located at different distances from the axis of
551 gallery r .

552 Figure 7: Void ratio of macro-pores e_M at different distances from the axis of gallery r .

553 Figure 8: SEM images viewing perpendicular (a) and parallel (b) to the bedding plane for the sample
554 located at $r = 2.5$ m; (a) picture scale: $1800 \times 1400 \mu\text{m}$ and (b) picture scale: $1500 \times 1100 \mu\text{m}$.

555 Figure 9: SEM images viewing perpendicular (a) and parallel (b) to the bedding plane for the sample
556 located at $r = 2.7$ m : (a) picture scale: $2550 \times 1950 \mu\text{m}$ and (b) picture scale: $850 \times 650 \mu\text{m}$.

557 Figure 10: SEM images viewing perpendicular (a) and parallel to the bedding plane (b) for the sample
558 located at $r = 9.2$ m: (a) picture scale: $2300 \times 1800 \mu\text{m}$ and (b) picture scale: $640 \times 500 \mu\text{m}$.

559 Figure 11: Comparison of hydraulic conductivity between the field measurements and model predictions.

560

561

Table 1: Physical and thermo-mechanical properties of natural Boom Clay. r : distance from the axis of gallery, w : water content (%), ρ : total density of the soil, λ : thermal conductivity, G : small-strain shear modulus, e : void ratio; e_M : void ratio of macro-pores.

Distance r (m)	w (%)	ρ (Mg/m ³)	e	λ_{\perp} (W/(m.K))	λ_{45} (W/(m.K))	$\lambda_{//}$ (W/(m.K))	G_{hv} (MPa)	G_{h45} (MPa)	G_{hh} (MPa)	e/e_M
2.5	20.7	1.97	0.65	0.898	1.267	1.341	807.85	1065.9	819.3	12.395
2.7	21.3	1.97	0.64	0.818	1.230	1.421	637.55	1369.3	1197.8	26.326
9.2	20.3	1.95	0.64	0.941	1.477	1.605	1206.77	1357.5	1197.8	67.107

Table 2: Parameters used for model predictions.

Property X	X_0
G_{hv} (MPa)	1100
G_{h45} (MPa)	1300
G_{hh} (MPa)	1450
V_p (m/s)	1930
$k_{\perp} \times 10^{-14}$ (m/s)	350
$k_{//} \times 10^{-14}$ (m/s)	650
$\lambda_{//} \times 10^{-3}$ (W/(m.K))	1650
$\lambda_{45} \times 10^{-3}$ (W/(m.K))	1500
$\lambda_{\perp} \times 10^{-3}$ (W/(m.K))	1100

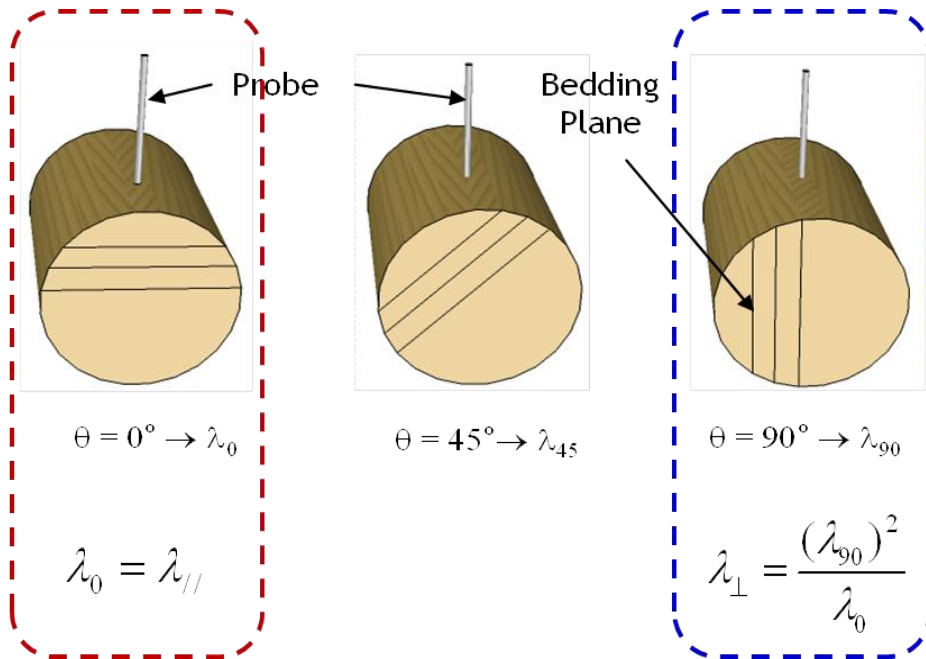


Figure 1: Measurement of thermal conductivity by needle probe method in the laboratory.

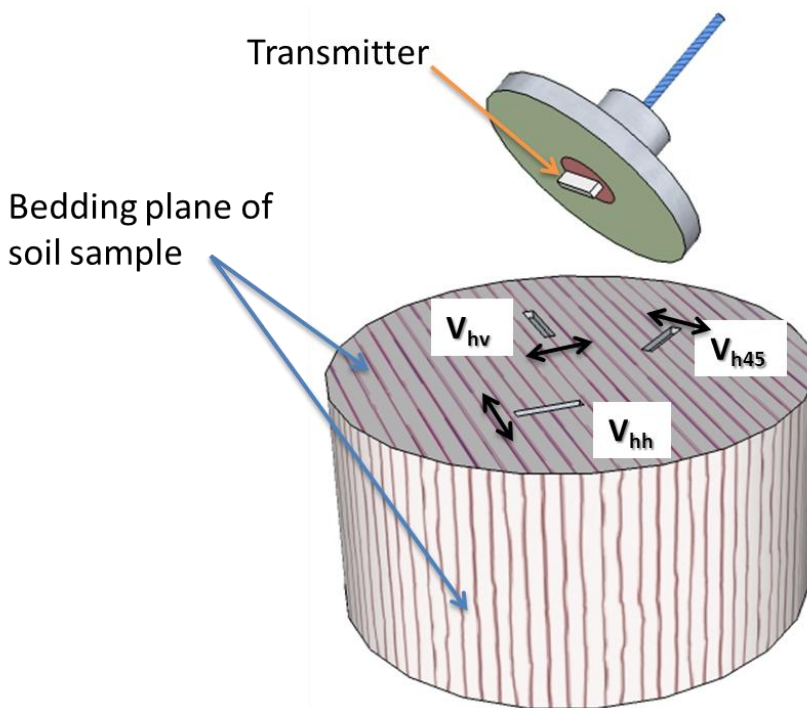
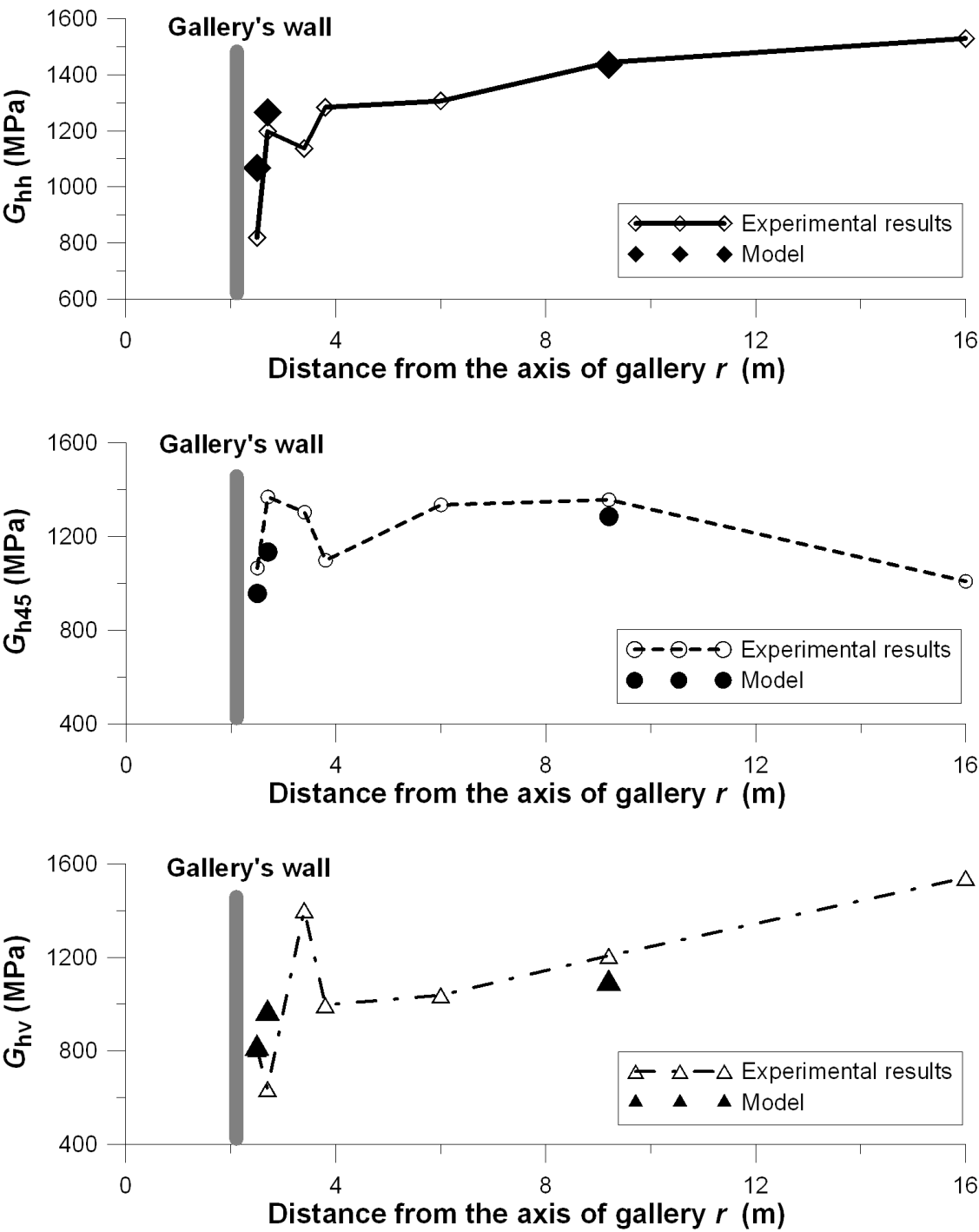


Figure 2: Measurement of shear wave velocity by bender element method in the laboratory (the three arrows indicate the directions of particle vibration).

590



591

592 Figure 3: Comparison of shear modulus between model and experiment.

593

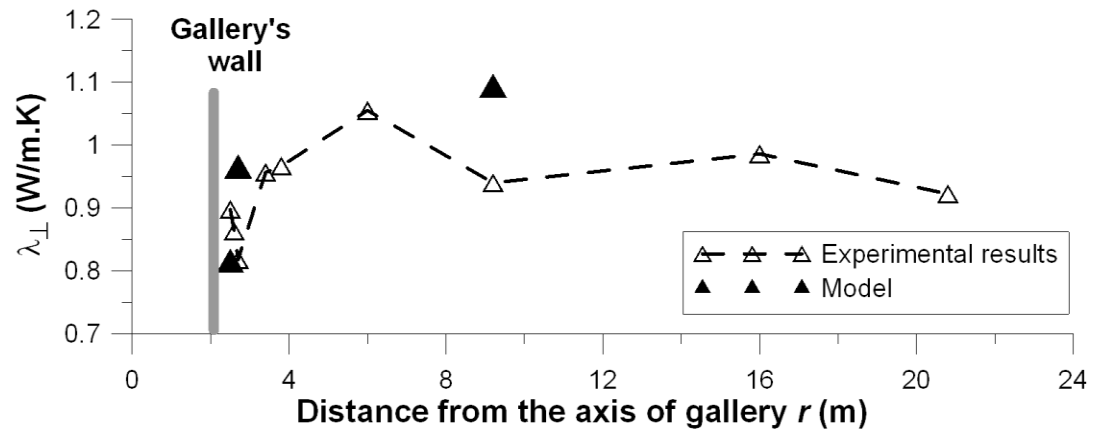
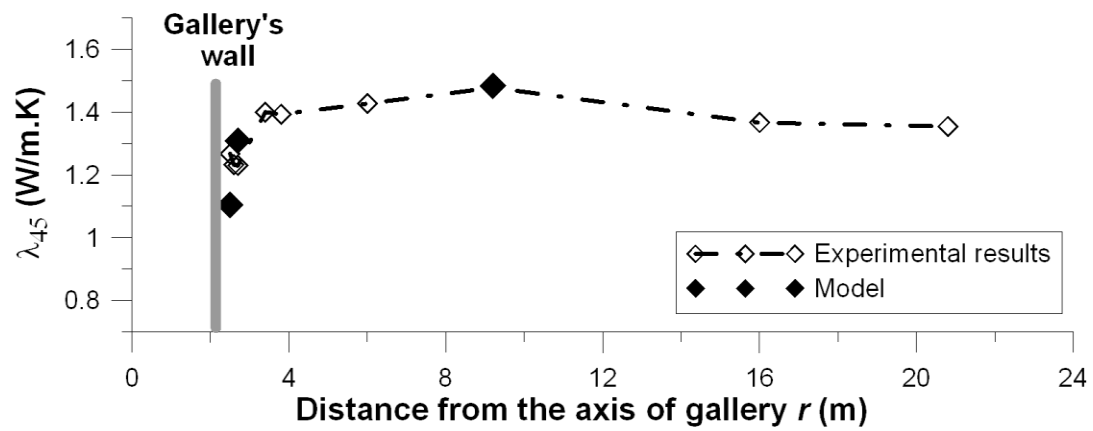
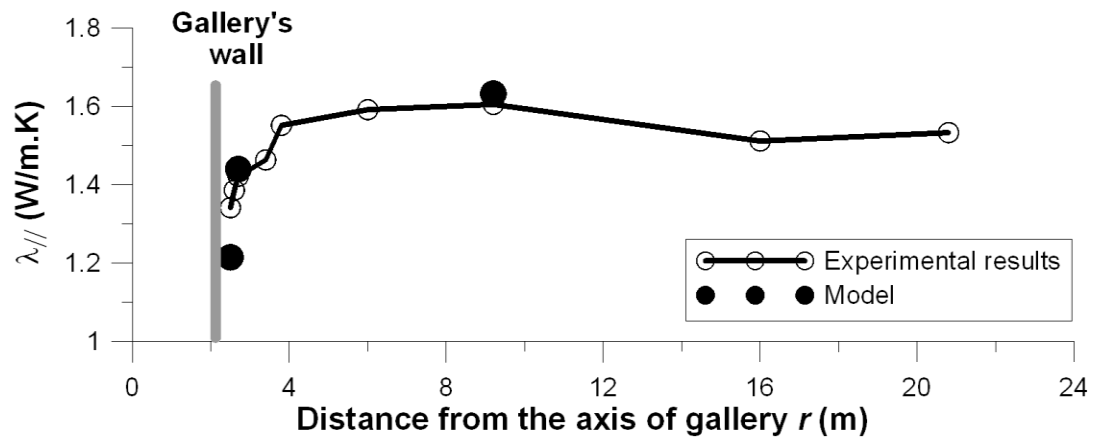


Figure 4: Comparison of thermal conductivity between model and experiment.



Figure 5: Bedding plane on natural Boom Clay sample.

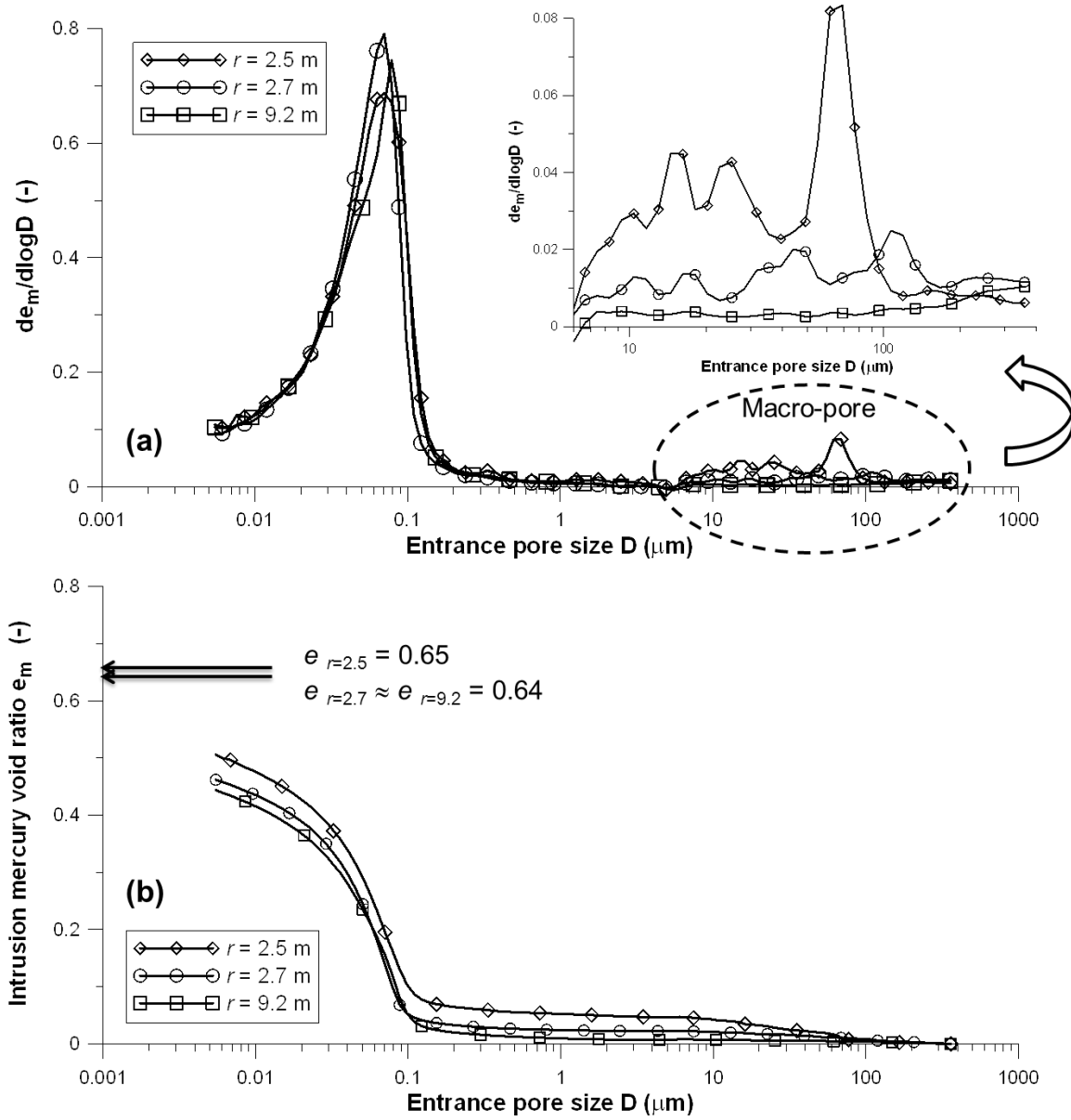
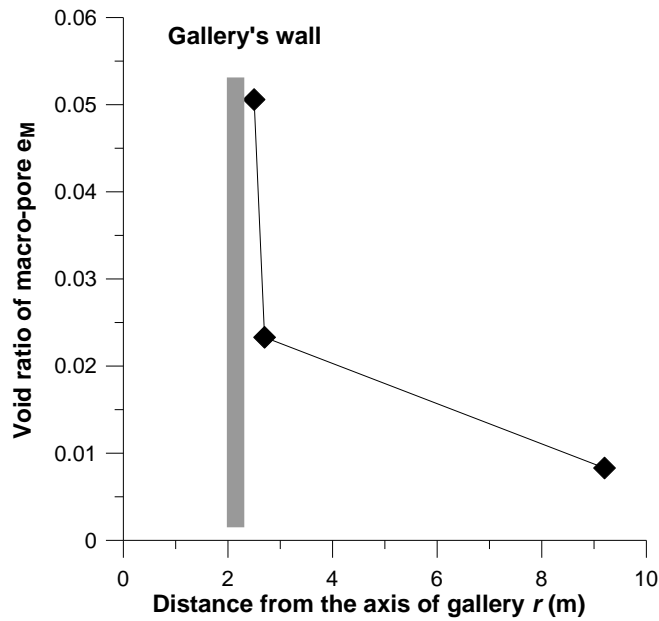


Figure 6: Pore size distributions of three Boom Clay samples located at different distances from the axis of gallery r .

607

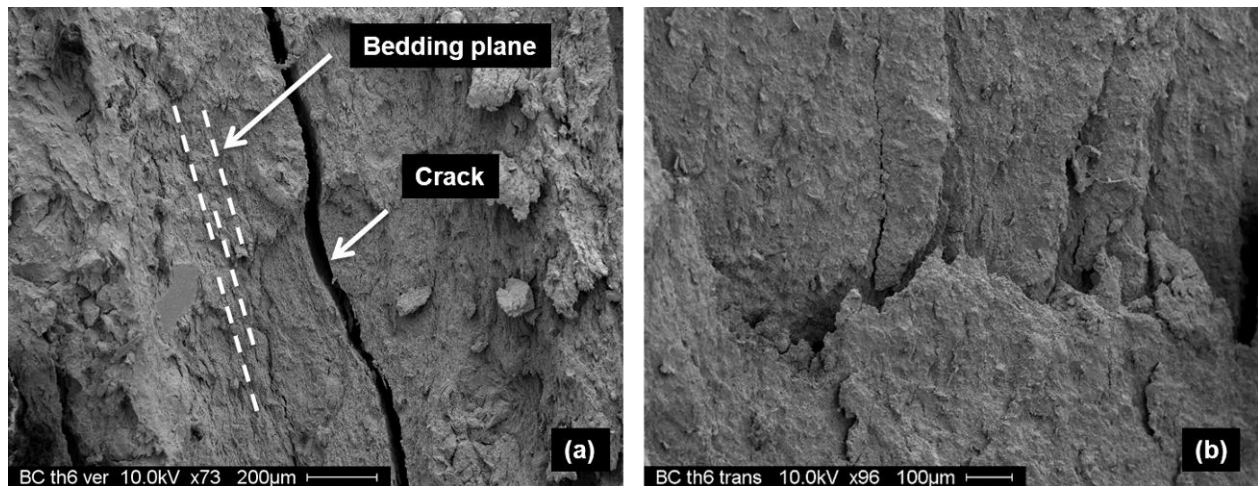


608

609 Figure 7: Void ratio of macro-pores e_M at different distances from the axis of gallery r .

610

611



612
613

614 Figure 8: SEM images viewing perpendicular (a) and parallel (b) to the bedding plane for the sample
615 located at $r = 2.5$ m; (a) picture scale: 1800 x 1400 μm and (b) picture scale: 1500 x 1100 μm .

616

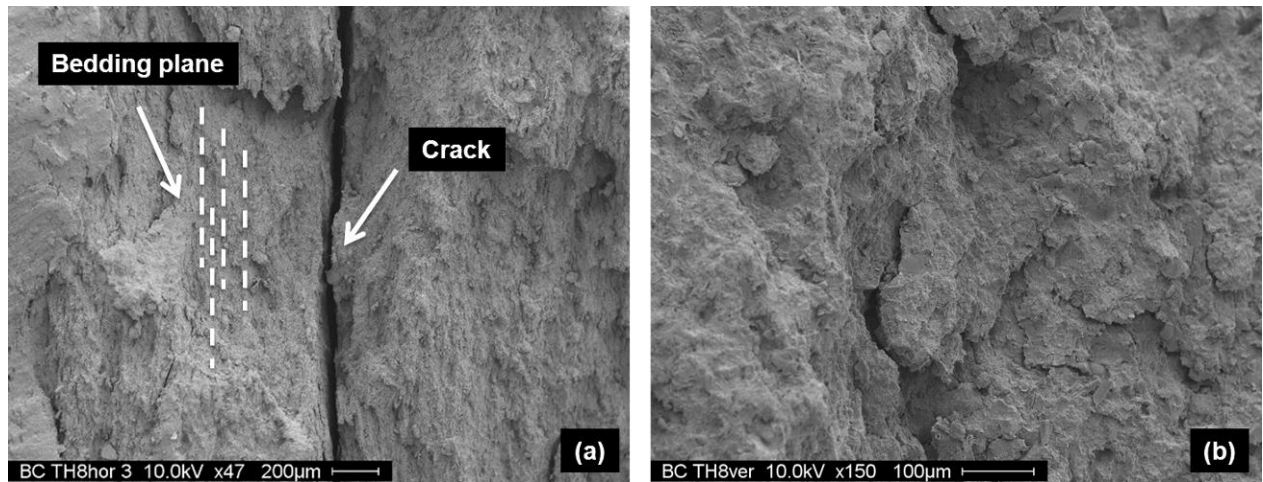


Figure 9: SEM images viewing perpendicular (a) and parallel (b) to the bedding plane for the sample located at $r = 2.7$ m : (a) picture scale: 2550 x 1950 μm and (b) picture scale: 850 x 650 μm .

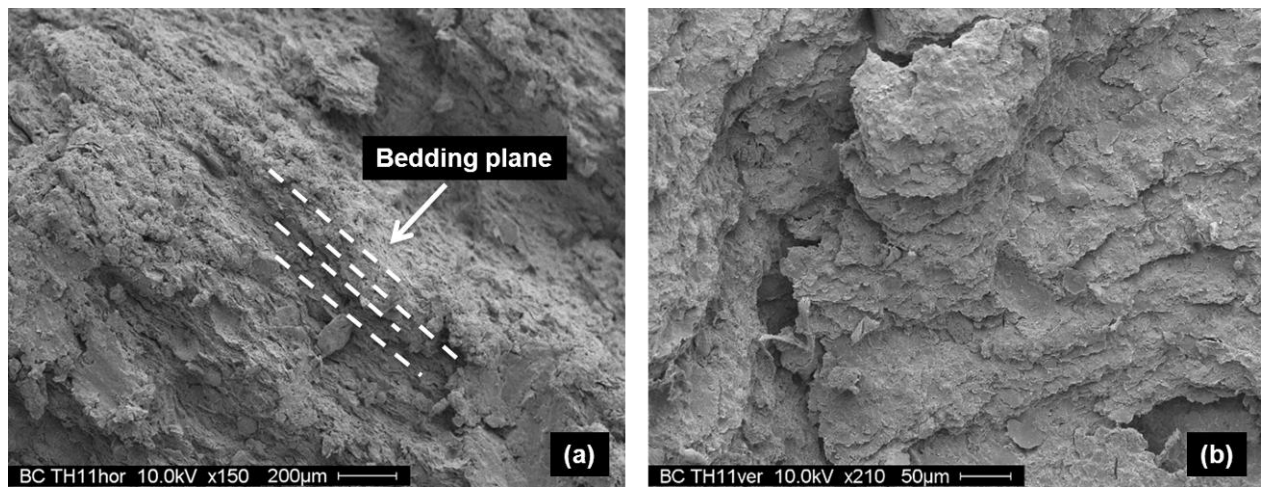


Figure 10: SEM images viewing perpendicular (a) and parallel to the bedding plane (b) for the sample located at $r = 9.2$ m: (a) picture scale: 2300 x 1800 μm and (b) picture scale: 640 x 500 μm .

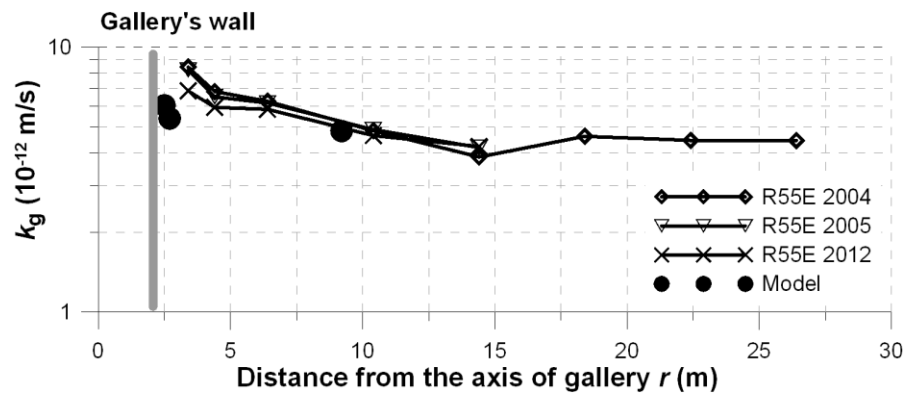
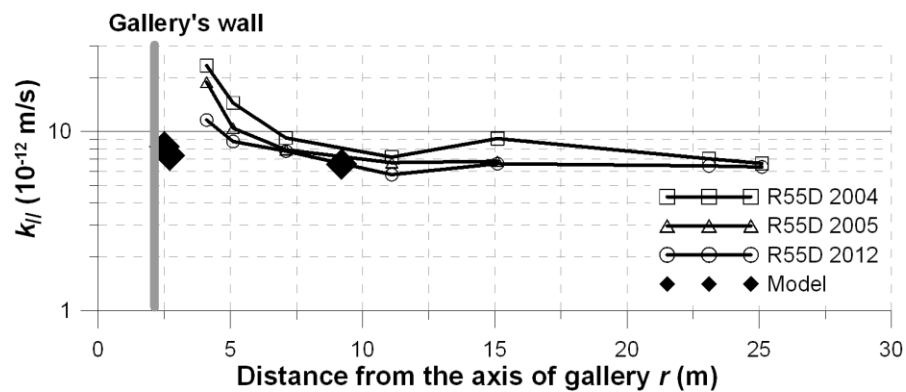


Figure 11: Comparison of hydraulic conductivity between the field measurements and model predictions.